Available online at www.sciencedirect.com
SCIENCE DIRECT®
Journal of Marine Systems 38 (2003) 287–303
JOURNAL OF MARINE SYSTEMS
www.elsevier.com/locate/jmarsys

# Hydrography and cohesive sediment modelling: application to the Rømø Dyb tidal area

U. Lumborg[a,*], A. Windelin[b]

[a] *Institute of Geography, University of Copenhagen, Øster Voldgade 10, DK-1350 Copenhagen K, Denmark*
[b] *Vejle County, Damhaven 12, DK-7100 Vejle, Denmark*

Received 30 April 2002; accepted 17 October 2002

**Abstract**

Estuaries act as sinks for fine-grained sediments and because of the cohesive properties of these sediments, heavy metals and nutrients tend to accumulate in estuaries. In order to quantify the erosion, transport and deposition of these pollutants, modelling of cohesive sediment dynamics is a very useful tool. However, the description of cohesive sediment dynamics through numerical analysis is a difficult task since the physical properties of cohesive sediments are of complex nature.

In this paper, setup and calibration of a cohesive sediment transport model covering the period from October 20, 1999 to December 13, 1999 are described and an interpretation of the results is carried out. Further, a comparison with measured suspended sediment concentrations and bed level measurements from the modelling period is presented.

A detailed bathymetry is used. This is necessary in order to describe the water movements in a realistic way. A bottom description is created in a way so that differences in erodibility of the sediment can be described. Further, a spatial differentiated description of critical shear stress, both for erosion and deposition of the cohesive sediment bottom, is made in order to describe the processes of settling and scour lag.

The hydrodynamic simulation is shown to be very reliable, and therefore, it has been possible to extract key values for the area. Thus, the maximum current velocities for the Lister Dyb area are modelled to 1.2 and 0.93 m $s^{-1}$ for the flood and ebb period, respectively. The tidal prism has likewise been computed to $620 \times 10^6$ $m^3$.

The cohesive sediment transport modelling has shown that the highest sediment concentrations at a given site appear when onshore winds are prevailing. Further, it can be recognized in the results that an inward sediment transport direction is prevailing, especially after a windy period with waves has mobilized considerable amounts of sediment.

A detailed investigation of the cohesive sediment's settling velocities collected in the area is used to give a site-specific description. Since the description of the settling velocity changes with temperature, several simulations using different descriptions have been carried out. These simulations have shown that this parameter is very influential for the net deposition result. Thus, an increase of the settling velocity will increase the deposition rates considerably.

The modelling results and the comparisons to measured data presented in this paper show that it has been possible to calibrate the hydrodynamic model in accordance with observed values. In continuation of this, the deformation of the tidal wave has also been modelled satisfactorily. Modelling of the cohesive sediment dynamics has been more complicated and the

* Corresponding author. Tel.: +45-35-32-25-45; fax: +45-35-32-25-01.
*E-mail address:* ul@geogr.ku.dk (U. Lumborg).

0924-7963/02/$ - see front matter 
PII: S0924-7963(02)00247-6

modelling results show divergence from the measured results. However, the levels of the sediment concentrations and the overall net sedimentation pattern show accordance with observed values.


*Keywords:* Hydrodynamics; Cohesive sediments; Sediment transport; Settling velocities; Modelling; Denmark; Lister Dyb tidal area

## 1. Introduction

The processes of flocculation, settling and scour lag, and the asymmetry of the tidal currents make cohesive sediment transport in estuaries difficult to forecast (Dyer, 1989; Teisson, 1991; van Leussen, 1994; Parker, 1997; Van der Lee, 2000). Because of the cohesive properties of the fine sediments, nutrients, heavy metals and other pollutive substances tend to bind to the sediment's surface (Rae, 1997). Consequently, pollutants can be concentrated in the estuaries, thus being of great environmental interest. In addition, the mudflats occurring in estuaries are important biotopes for a large number of micro- and macro-faunal species and act as feeding places for a number of birds (Eisma, 1998). This makes forecast of erosion, transport and deposition of cohesive sediment of great interest in estuaries.

Because of this, modelling of the dispersion of cohesive sediments will be of major importance in the future, and numerical simulation models will have a great potential when it comes to estimation of the effects of dredging of ports, building of dams, discharge of environmental pollutants and the global eustatic sea level rise. These simulation models can make it possible to quantify the sediment erosion, transport and deposition over a large area during a given period. The results can be investigated at time scales down to e.g. 5-min intervals. This combination of features can hardly be obtained by the use of traditional in situ measurements. Still, the fieldwork is the basis for the development of the model and fieldwork is required in order to calibrate and validate the model. The use of fieldwork and modelling can therefore be an extremely profitable combination.

The now-existing cohesive sediment transport models all use an advection–dispersion equation to simulate the cohesive sediment transport in the water column (e.g. Teisson, 1997). The advection–dispersion equation requires current velocity components and water levels that are normally provided from a decoupled hydrodynamic model. The models have further incorporated a variety of equations that describe the cohesive sediment erosion, flocculation and deposition processes in different ways (e.g. Mehta et al., 1989; Teisson, 1991). However, most papers that describe setups of cohesive sediment transport models (e.g. Cancino and Neves, 1999; Le Normant, 2000) only present very short time series (hours or few days). If a realistic extrapolation of modelling results in time and space should be carried out, longer time series with a high degree of truthfulness needs to be obtained. This first requires a very well-calibrated hydrodynamic model. Hereafter, a profound calibration of the cohesive sediment transport model going thoroughly through each of the calibration parameters must be carried out.

In the future, there will be a need for comprehensible sediment transport models and the demand for reliability will further increase.

In this research project, it was attempted to set up and calibrate a numerical model so that the sediment transport is described satisfactorily, and further, to model cohesive sediment transport in a Danish estuary over a period of several weeks.

This paper describes the setup of a state-of-the-art sediment transport model (MIKE 21 MT) for the Rømø Dyb tidal area in the Danish Wadden Sea. The model is used for hindcast of sediment transport. The paper includes an analysis of the results and a comparison to previously published research from the area and theoretical aspects of cohesive sediment transport.

## 2. Study area

The Lister Dyb tidal area is situated in the northern part of the European Wadden Sea. The barrier islands Rømø and Sylt protect it from the North Sea

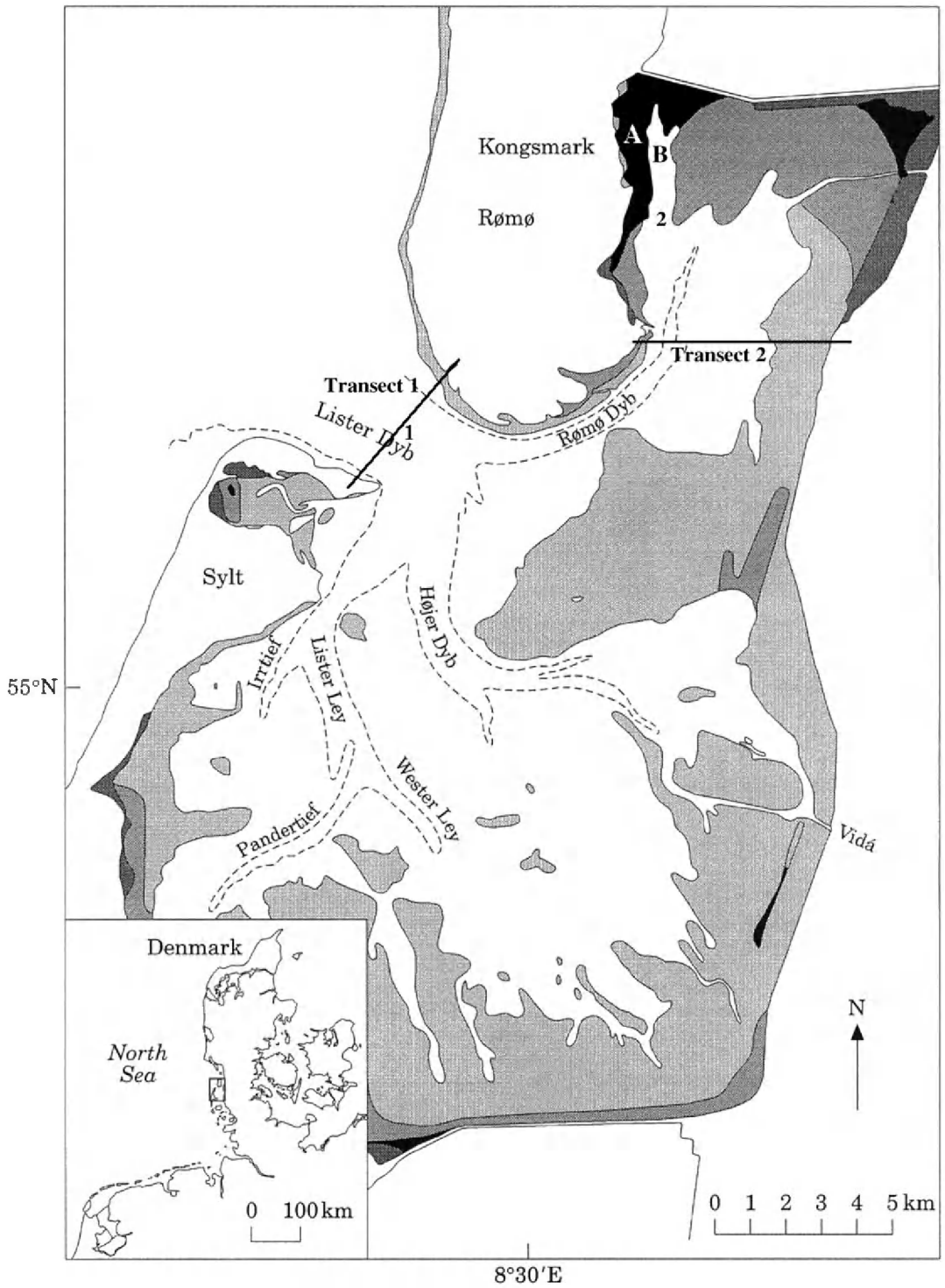


Fig. 1. Map of study area. Positions for sea truth data and positions for further analysis of hydrodynamic and sediment key values are indicated. The map is based on Pejrup et al. (1997). Legend: black = mud flat; dark grey = salt marsh; grey = mixed mud flat; light grey = sand flat; white = subtidal.

(Fig. 1). Lister Dyb tidal compartment covers an area of approximately 400 $km^2$, and the tide is semi-diurnal with a mean range of 1.8 m (Pejrup et al., 1997). To the north, the area is restricted by the Rømø Dam and to the south by the Hindenburg Dam. The only connection to the North Sea is through Lister Dyb, having a mean depth varying between 20 and 30 m.

Dynamically, the Lister Dyb tidal area is micro-tidal (Davies, 1964) or lower meso-tidal (Hayes, 1979) with two small fresh-water sources, the rivers Brede Aa and Vidaa. After the physiographic classification (Pritchard, 1960), the area can be classified as a bar built estuary, and from the morphogenetic classification, it is a choked coastal lagoon (Perillo, 1995).

The Lister Dyb tidal area is drained by three minor tidal channels Lister Ley, Højer Dyb and Rømø Dyb. The main tidal channel Lister Dyb collects the three minor tidal channels. A minor part of the Lister Dyb tidal area consists of tidal mud flats that are inundated nearly every flood tide. Under normal weather conditions, the tidal flats are covered with water for a period of 4.5–8 h during each tidal period (Andersen, 1999).

The distribution of the bottom sediment on the intertidal flats in the Lister Dyb tidal area has been investigated both by Bayerl et al. (1998) and Pejrup et al. (1997) (Fig. 1). These investigations define the intertidal flats into three groups: sand flats (>95% sand), mixed mud flats (10–50% sediment < 63 μm) and mud flats (>50% sediment < 63 μm). Further, Pejrup et al. (1997) have estimated the accumulation of fine-grained sediment (< 63 μm) on the basis of $^{210}$Pb-dating. This accumulation amounts to 58 000 ton $year^{-1}$. In the same study, a sediment budget has been calculated, where the inputs of fine-grained sediment are fluvial input, 14%; biological production, 15%; erosion of salt marsh, 5%; atmospheric sedimentation, 2%. The input from the North Sea is then estimated to 64% of the total sedimentation in the Lister Dyb tidal area. Postma (1981) has estimated that only about 5% of the input of fine-grained sediment from the North Sea to the Wadden Sea is actually deposited. If this remains true, it means that about 740 000 tons of suspended sediment is circulated to and from the area each year. The fine-grained cohesive sediment has a median primary grain size of about 10 μm consisting of about 50% montmorillonite, 30% illite and 20% kaolinite (Edelvang, 1996).

## 3. Methods

The MIKE 21 modelling system (DHI, 1999a) has been set up for the Lister Dyb tidal area for the period from October 20, 1999 to December 13, 1999. This 7-week period thus covers a typical Danish autumn situation with both windy and calm periods. Further, an extreme storm situation occurred on December 3, 1999.

In the first place, a hydrodynamic modelling of the Lister Dyb tidal area and a part of the North Sea (Fig. 1) has been made using the model MIKE 21 HydroDynamic (HD module) (DHI, 1999a). Afterwards, another hydrodynamic model has been made covering only the Rømø Dyb tidal area. This area was used for further studies including modelling of the fine-grained sediment erosion, transport and deposition. The sediment transport has been modelled using the model MIKE 21 Mud Transport (MT module). Furthermore, because of the very important influence the waves have on the erosion of the sediment (e.g. Janssen-Stelder, 2000), a number of wave fields, each having unique values of water level, wind direction and wind velocity, have been modelled using the model MIKE 21 Near Shore Waves (NSW module) (DHI, 1999b). These wave fields are incorporated into a three-dimensional wave database. At each time step in the model, an interpolation in this database is made in order to obtain a time-specific wave field, and in this way, the effect of wind waves is simulated.

The hydrodynamic model in MIKE 21 is a numerical modelling system for the simulation of water levels and flows in estuaries, bays and coastal areas. It simulates unsteady two-dimensional flows in one-layer (vertically homogeneous) fluids. The hydrodynamic simulations are used as a basis for the add-on modules like the mud transport module MIKE 21 MT.

The near shore waves module MIKE 21 NSW is a wind-wave model which describes the propagation, growth and decay of short-period waves in near shore areas. The model includes the effects of refraction and

shoaling due to varying depth, wave generation due to wind and energy dissipation due to bottom friction and wave breaking. The effects of currents on these phenomena are included by using the equations from Holthuijsen et al. (1989) from the conservation equation for the spectral wave action density. The assumptions of using the module as well as a detailed description of the governing equations are presented in Johnson (1998).

The mud transport module used is essentially based on the formulas given in Mehta et al. (1989) and includes description of sediment settling with different settling velocities (flocculation), hindered settling and a combination of currents and waves to calculate the bottom shear stress. The module can be applied in areas where a large part of the sediment has cohesive properties like in many estuaries. A brief description of the formulas is given in the following and a flow chart is presented in Fig. 2.

Transport of the suspended sediment is calculated using the advection–dispersion equation which is classically written (e.g. Teisson, 1991):

$$\frac{\overline{\partial c}}{\partial t} + V_X \frac{\overline{\partial c}}{\partial x} + V_Y \frac{\overline{\partial c}}{\partial y} = \frac{1}{h}\frac{\partial}{\partial x}\left(hD_X \frac{\overline{\partial c}}{\partial x}\right) + \frac{1}{h}\frac{\partial}{\partial y}\left(hD_Y \frac{\overline{\partial c}}{\partial y}\right) + \sum_{i=1}^{n} \frac{S_i}{h} \quad (1)$$

where $c$ is the depth averaged suspended sediment concentration (g m$^{-3}$), $V_X$ and $V_Y$ are depth averaged flow velocities (m s$^{-1}$) (calculated in the hydrodynamic module), $D_X$ and $D_Y$ are dispersion coefficients (m$^2$ s$^{-1}$), $h$ is water depth (m) (calculated in the hydrodynamic module) and $S_i$ is the source/sink term (g m$^{-2}$ s$^{-1}$). This term accounts for the deposition or erosion that is calculated in Eqs. (4) and (6), respectively (see below).

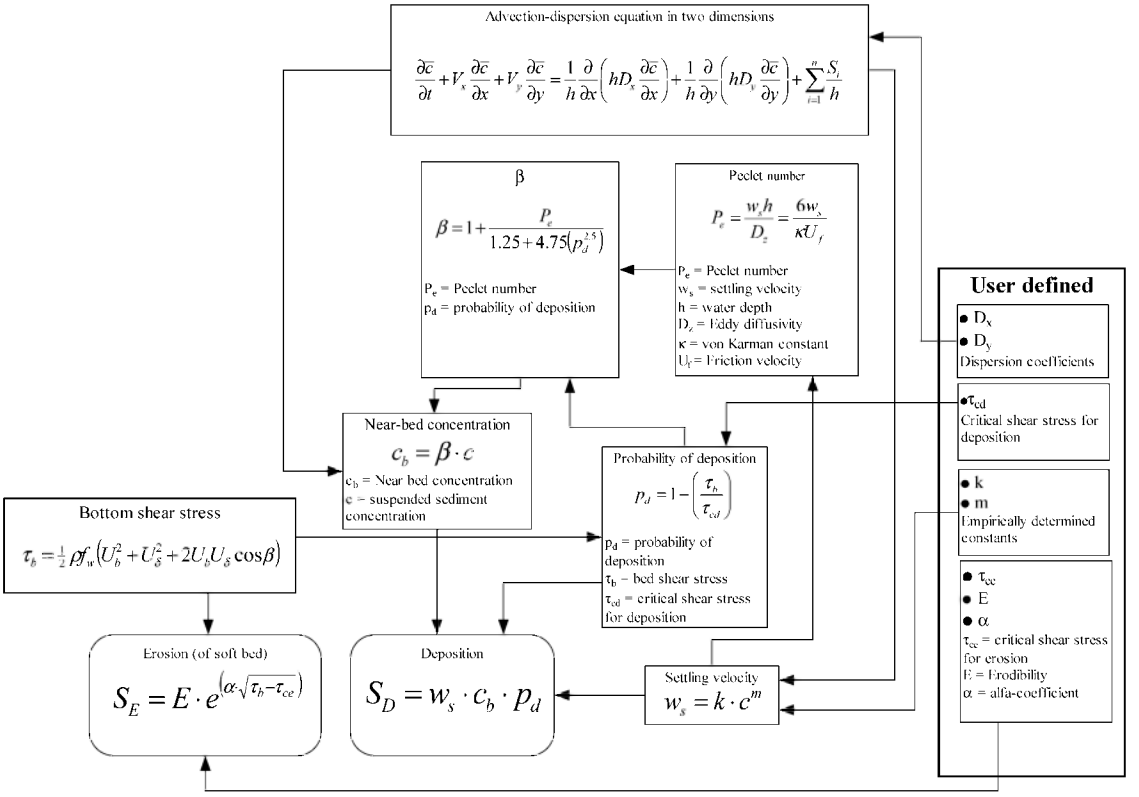


Fig. 2. Flow chart showing all MT variables and their interdependencies. See text for explanations on each parameter.

The bottom shear stress ($\tau_b$ in N m$^{-2}$) is calculated with respect to currents and waves using the following equation:

$$\tau_b = \frac{1}{2}\rho_w f_w \left(U_b^2 + U_\delta^2 + 2U_b U_\delta \cos\beta\right) \quad (2)$$

where $\rho_w$ is the density of water (kg m$^{-3}$), $U_b$ is the horizontal mean wave orbital velocity at the bed (m s$^{-1}$), $U_\delta$ is the current velocity at the top of wave boundary layer (m s$^{-1}$), $\beta$ is the angle between the mean current direction and the direction of wave propagation and $f_w$ is a wave friction factor. The wave friction factor is approximated by:

$$f_w = \exp\left(5.213\left(\frac{a}{k_b}\right)^{-0.194} - 5.977\right) \quad (3)$$

where $a$ is the horizontal mean wave orbital motion at the bed (m) and $k_b$ is the bed roughness (m). $U_b$, $U_\delta$, $a$ and $\beta$ are calculated by the near shore waves module. The model derives $U_\delta$ from depth averaged current velocities calculated in the hydrodynamic module.

The formula of deposition (Eq. (4)) is originally proposed by Krone (1962) and has a stochastic element incorporated, since the $p_d$ part is the probability of deposition which is dependent on the ratio between the bottom shear stress ($\tau_b$) and the critical shear stress of deposition ($\tau_{cd}$) (see Fig. 2). The near bottom concentration ($c_b$, in g m$^{-3}$) is dependent on the depth averaged sediment concentrations as described in Teeter (1986) (see Fig. 2).

$$S_D = w_s c_b p_d \quad (4)$$

where $S_D$ is the deposition rate in g m$^{-2}$ and $w_s$ is the sediment's settling velocity in m s$^{-1}$.

The settling velocity in m s$^{-1}$ ($w_s$) is described by the well-known exponential relationship with the suspended sediment concentration as shown by Burt (1986) and Pejrup (1988).

$$w_s = kc^m \quad (5)$$

where $k$ and $m$ are site-specific constants that have to be determined empirically.

Erosion from the sediment bed is described using an expression originally proposed by Parchure and Mehta (1985). The expression for erosion is as follows:

$$S_E = E e^{\left|\alpha\sqrt{\tau_b - \tau_{ce}}\right|} \quad (6)$$

where $S_E$ is the erosion rate in g m$^{-2}$, $E$ is the erodibility of the bed (g m$^{-2}$ s$^{-1}$), $\tau_{ce}$ is the critical shear stress for erosion (N m$^{-2}$) and $\alpha$ is the erosion coefficient (m N$^{-0.5}$).

The model setup has been focused on estimating the different site-specific parameters required. For the description of the vertical variation of the bottom's physical characteristics, a model consisting of six unique layers was chosen. Further, the characteristics of these layers have been varied horizontally in order to describe the different erosion and deposition characteristics that occur in the area.

Additionally, a number of parameters describing the settling velocity, the deposition and the erosion processes were measured in the area or estimated based on literature. The most important parameters are presented in the following and a complete overview of the input parameters is shown in Tables 1 and 2.

The settling velocity of the suspended sediment is shown to be dependent on the suspended sediment concentration and the shear stress in the water column (Dyer, 1989). However, no significant relationship that relates to both the concentration and the shear

Table 1
Inputs for bottom layers in MIKE 21 MT

| Layer no. | Density of bottom sediment (g m$^{-3}$) | $\tau_{ce}$ (N m$^{-2}$) | $T_i$ (g m$^{-2}$ s$^{-1}$) | $E$ (g m$^{-2}$ s$^{-1}$) | $\alpha$ (m N$^{-0.5}$) | Initial thickness (mm)[a] |
|---|---|---|---|---|---|---|
| 1 | 90 000 | 0.2 | 0.001 | 0.005 | 6.5 | 0–5 |
| 2 | 129 000 | 0.3 | 0.001 | 0.005 | 6.5 | 0–50 |
| 3 | 225 000 | 0.4 | 0.001 | 0.005 | 6.5 | 0–20 |
| 4 | 300 000 | 0.5 | 0.0001 | 0.005 | 6.5 | 0–50 |
| 5 | 450 000 | 0.7 | 0.0001 | 0.005 | 6.5 | 2–50 |
| 6 | 600 000 | 1.5 | | 0.005 | 6.5 | 400 |

[a] The thicknesses vary spatially over the area.

Table 2
Overview of other input data in MIKE 21 MT

| Parameter | Value |
|---|---|
| *Initial parameters and bottom description* | |
| Background concentration | 30 mg $l^{-1}$ |
| Boundary concentration | 30 mg $l^{-1}$ |
| Suspended sediment concentration at the source (Brede Aa) | 20 mg $l^{-1}$ |
| Bed roughness ($z_0$) | 0.001 m |
| Critical bottom shear stress for deposition ($\tau_{cd}$)[a] | 0.0002–1 N $m^{-2}$ |
| *Settling velocity ($w_s$)* | |
| $0 \le c \le 6$ mg $l^{-1}$ | $3 \times 10^{-5}$ m $s^{-1}$ |
| $6 < c \le 400$ mg $l^{-1}$ | $3.96 \times 10^{-6} \times c^{1.19}$ m $s^{-1}$ |
| $c > 400$ mg $l^{-1}$ | 0.005 m $s^{-1}$ |
| *Dispersion coefficients (proportional to the current)* | |
| $D_X$ | 15 m $s^{-1}$ |
| $D_Y$ | 15 m $s^{-1}$ |
| $D_{min}$ | 1 m $s^{-1}$ |
| $D_{max}$ | 16 m $s^{-1}$ |

[a] Varies spatially over the area.

stress has been obtained in the Rømø Dyb tidal area (Mikkelsen and Pejrup, submitted for publication). Therefore, a large set of data collected in the study area during the last 10 years has been analyzed. The settling velocity has been measured and analyzed using a Braystroke SK-110 settling tube (e.g. Pejrup and Edelvang, 1996). The measurements relate the settling velocity to suspended sediment concentration. For a typical autumn situation, these data suggest the relationship $w_s = 3.96 \times 10^{-6} \times c^{1.19}$ with an $R^2$ value of 0.80.

The critical shear stress for erosion ($\tau_{ce}$) is a required value for setting up the model. The parameter has been measured in the study area by Austen et al. (1999) who found values in the interval 0.16–3 N $m^{-2}$. The greater part of the explanation for the variations is the inundation length of the intertidal flats. Therefore, the model setup has concentrated on choosing the $\tau_{ce}$-values controlled by the bottom elevation, inundation time and the sediment characteristics. The values applied in this study vary from 0.1 to 0.7 N $m^{-2}$. A value of 1.5 N $m^{-2}$ is applied to the lowest bottom layer in order to artificially prevent erosion from this layer.

The critical shear stress for deposition ($\tau_{cd}$) has not been measured in the Rømø Dyb tidal area, so this parameter has been used as a calibration factor. However, literature values originating from laboratory studies have been found to support the calibration. Krone (1962) found $\tau_{cd}$-values at 0.06–0.078 N $m^{-2}$ and Mehta and Partheniades (1975) found values at 0.18–1.1 N $m^{-2}$. The values applied in this context vary in the study area from 0.002 to 1.0 N $m^{-2}$. The variations in $\tau_{cd}$ are due to the different sediment characteristics in the area (see Fig. 1).

The erosion coefficient ($E$) is a calibration factor used to control the overall level of the erosion (Eq. (6)). The erosion coefficient has been calibrated to 0.005 g $m^{-2}$ $s^{-1}$ for all six bottom layers. Parchure and Mehta (1985) state values of 0.0067–0.3 g $m^{-2}$ $s^{-1}$ and van Rijn (1989) has values varying from 0.0005 to 0.005 g $m^{-2}$ $s^{-1}$.

The $\alpha$ coefficient is a calibration coefficient that steers the exponential rise in erosion when $\tau_b$ rises. The coefficient has been calibrated to 6.5 m $N^{-0.5}$ for all six bottom layers. Parchure and Mehta (1985) state values of the $\alpha$ coefficient from different studies to be between 4.2 and 25.6 m $N^{-0.5}$ and van Rijn (1989) estimates values from 10 to 20 m $N^{-0.5}$.

The parameters that were measured in the area (settling velocity and critical shear stress for erosion) have not been changed during the model set-up. However, the calibration factors critical shear stress for deposition, erosion coefficient and $\alpha$ coefficient have been varied in different combinations until a realistic erosion pattern was obtained.

Consolidation of the bottom sediment is not directly included in the model. However, a transition coefficient ($T_i$) can be used to determine a rate at which the sediment from upper layers is transformed to sediment at lower layers. As the layers have different characteristics as critical shear stress for erosion, the sediment will have a higher critical bottom shear stress for erosion after successively longer residence times.

The bathymetry used for the simulations has been provided from the Danish Coastal Authorities. Measurements have been made with a spatial interval of 2 m and the accuracy has been estimated to $\pm 5$ cm (Danish Coastal Authorities). The grid for the setup concerning the Lister Dyb tidal area was 150 m. For the Rømø Dyb tidal area, the grid size was chosen to be 50 m in order to give a more detailed description of the hydrodynamics and sediment transport processes.

Wind data needed to simulate the hydrodynamics and the wave fields were provided by the Danish Meteorological Institute, who measures wind speed, wind direction and pressure at the village Juvre on Rømø every hour.

During the period, two self-recording Aanderaa RCM 9 current meters were used, measuring water depth, current velocity, current direction and suspended sediment concentration. One RCM 9 meter was located in a tidal channel and the other one was located on an intertidal flat near the village Kongsmark on Rømø. The positions for the two current meters are indicated in Fig. 1. Unfortunately, the current meter placed on the tidal flat was malfunctioning and therefore only provided data for the first 2 weeks of the simulation period. The data from these current meters were used for calibration and validation of the model. Data from the first month were used for calibration while data from the last 3 weeks were used for validation of the modelled results.

## 4. Results and discussion

### 4.1. Hydrographic conditions

When it comes to the modelling of cohesive sediment transport, it is a prerequisite that the hydrodynamic conditions in the area are representative for the actual occurring water currents in the area (Teisson, 1991). This part of the paper demonstrates the quality of the hydrodynamic simulation. A comparison of measured and simulated water levels for a typical period is shown in Fig. 3.

Table 3
Hydrodynamic values for the Lister Dyb tidal compartment (including the Rømø Dyb tidal area)

| Parameter | Lister Dyb (point 1) | Rømø Dyb (point 2) | Tidal flats (point A) |
|---|---|---|---|
| $V_{max}$ (ebb) | 1.20 m $s^{-1}$ | 1.15 m $s^{-1}$ | 0.3–0.4 m $s^{-1}$ |
| $V_{max}$ (flood) | 0.93 m $s^{-1}$ | 0.96 m $s^{-1}$ | 0.3–0.4 m $s^{-1}$ |
| $V_{50}$ (ebb) | 0.59 m $s^{-1}$ | 0.56 m $s^{-1}$ | – |
| $V_{50}$ (flood) | 0.50 m $s^{-1}$ | 0.46 m $s^{-1}$ | – |
| $Q_{max}$ (ebb) | 57 600 $m^3$ $s^{-1}$ | 6600 $m^3$ $s^{-1}$ | – |
| $Q_{max}$ (flood) | 61 000 $m^3$ $s^{-1}$ | 6100 $m^3$ $s^{-1}$ | – |

Results relating to the hydrodynamic modelling in the Lister Dyb tidal compartment (including Rømø Dyb tidal area) will be presented in following. The values are based on numerical simulations with MIKE 21 HD, representing a period of 7 weeks. In Fig. 3, observed and simulated water levels are shown for a typical period and some key average values from the model simulations are presented in Table 3. These values should be seen as typical values for the area. The values are in the same order as the previously reported results from the area (Andersen, 1999; Andersen and Pejrup, 2001; Backhaus et al., 1998;

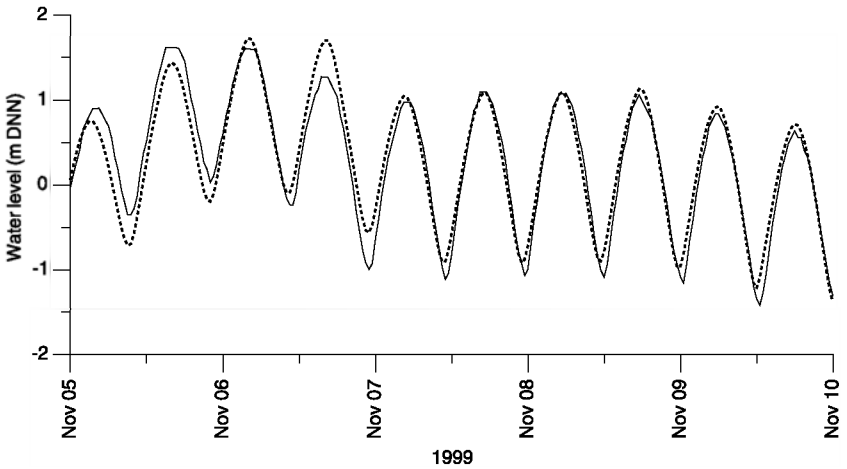


Fig. 3. Comparison of measured and observed water levels at calibration point B. Legend: (—) observed water levels; (----) simulated water levels.

Møller and Mikkelsen, 1997). It is believed that the hydrodynamic model is well calibrated and that the modelled results are very close to the actually occurring water movements. The locations and the cross-sections for the hydrodynamic values in Table 3 are indicated in Fig. 1.

Based on the model simulations, the tidal height at Havneby is 1.8 m. The highest water elevation was 3.53 m DNN (Danish Ordnance Datum) during the storm of December 3, 1999 and the lowest modelled water elevation is −2.12 m DNN. This low water level is connected to a longer period with easterly winds. These values are in good accordance with measured water levels from the same period.

In Rømø Dyb, the mean current velocities are calculated to 0.46 m $s^{-1}$ for the flood current and 0.56 m $s^{-1}$ for the ebb current. The maximum flood current velocity is found to be 0.96 m $s^{-1}$ while the corresponding value for the ebb current is 1.15 m $s^{-1}$. Møller and Mikkelsen (1997) report maximum current velocities at 0.67 and 0.56 m $s^{-1}$ for the flood and ebb period, respectively. In Lister Dyb, the mean current velocity for the flood period amounts to 0.5 m $s^{-1}$ and the parallel value for the ebb period is found to be 0.59 m $s^{-1}$. The maximum current velocities for Lister Dyb are found to be 1.2 m $s^{-1}$ for the flood period and 0.93 m $s^{-1}$ for the ebb period. Backhaus et al. (1998) report a maximum current velocity of 1.3 m $s^{-1}$.

One of the most characteristic hydrodynamic features in estuaries is the deformation of the tidal wave, and consequently, the asymmetry of the current velocities. This is illustrated for the Lister Dyb tidal area in Fig. 4, where modelled results of water elevation and current velocity are shown for three points in the area. It can be seen that the high water at the Kongsmark site is appearing 20–30 min after it has appeared in Lister Dyb. Further, the low water

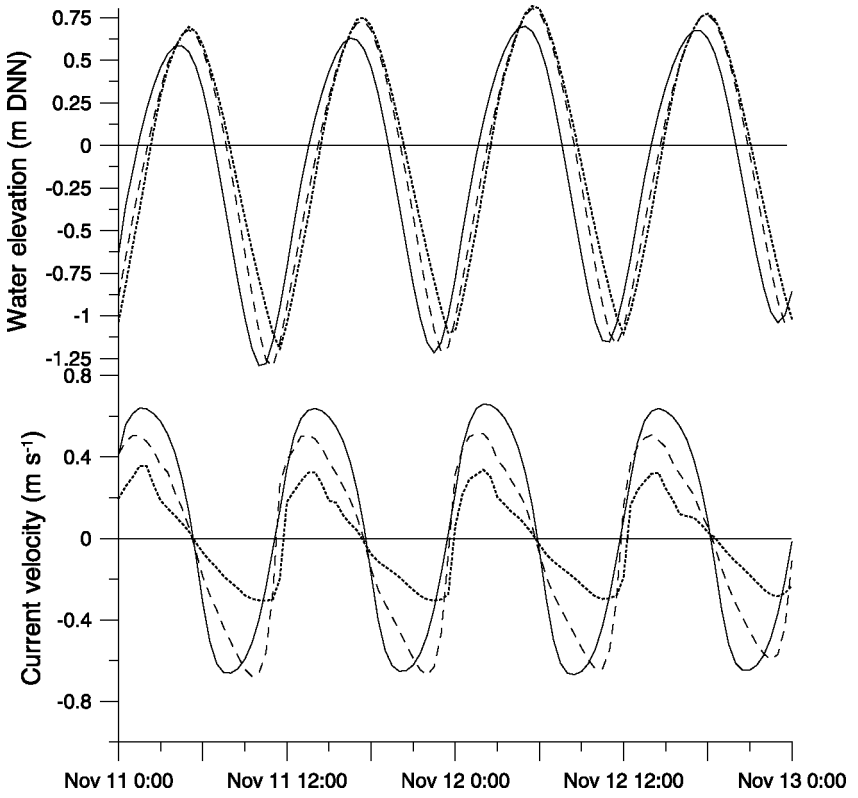


Fig. 4. Simulated water levels and current velocities illustrating the deformation of the tidal wave through the study area. Legend: (—) Lister Dyb (main tidal channel; point 1); (----) Fuglegrøft (tidal channel; point 2); (·····) Kongsmark (outer tidal flat; point A).

at Kongsmark is appearing 1–1.5 h after the low water in Lister Dyb.

The asymmetry of the tidal wave appears because the tidal wave crest due to bottom friction moves faster than the trough. This leads to a shorter flood period and a longer ebb period. Because of the law of mass conversation, the flood current velocities become greater than the ebb current velocities and thus favoring an inward sediment transport. This transport direction is further emphasized by the settling/scour lag processes (van Straaten and Kuenen, 1958).

The water discharge has been calculated in Lister Dyb. The highest modelled water discharges have been found to be 61 000 $m^3\ s^{-1}$ for the flood current and 57 500 $m^3\ s^{-1}$ for the ebb current. These discharges are slightly higher than earlier findings from the area (Fanger et al., 1998), but can be explained by the extreme storm occurring on December 3, 1999. When results from the storm are omitted from the calculations, the maximum discharges are found to be approximately 40 000 $m^3\ s^{-1}$, which is in agreement with the values reported in Fanger et al. (1998).

The tidal prism for the Lister Dyb tidal area has been calculated in two ways. The first one has been calculated from the model simulations of water fluxes. The other one has been calculated from a hypsographic curve (Fig. 5), where the used mean sea level was 0.22 m DNN as reported by the Danish Coastal Authorities. The two methods have given about the same results, respectively, $622 \times 10^6$ $m^3$ (model simulations) and $621 \times 10^6$ $m^3$ (hypsographic curve; Fig. 5).

The size of the tidal prism is quite different from earlier findings, where the tidal prism is found to be $530 \times 10^6$ (Lundbak, 1945) and $520 \times 10^6$ $m^3$ (Fanger et al., 1998). The explanations for the discrepancy between the earlier findings and the here-presented result are described in following.

The value $520 \times 10^6$ $m^3$ reported in Fanger et al. (1998) is made by extrapolating a water discharge of 23 000 $m^3\ s^{-1}$ measured in the middle of the tidal period. This water discharge was measured on 2 days of fieldwork. The large difference from the result presented in this study may relate to the position of the measurements and to the meteorological circumstances on the 2 days of fieldwork; therefore, the method applied by Fanger et al. (1998) is not well suited for measuring tidal prisms.

Lundbak (1945) denotes a value of $530 \times 10^6$ $m^3$ from 1 day of fieldwork and postulates that the weather conditions that day were representative as a normal day. Further, he presents data for producing a hypsographic curve. The difference comes from that he uses a mean water level at 0.075 m DNN. The mean water level measured during the last 30 years is 0.22 m DNN as reported by the Danish Coastal Authorities. Thus, the water level rise accounts for $61.5 \times 10^6$ $m^3$. The remaining difference may be due

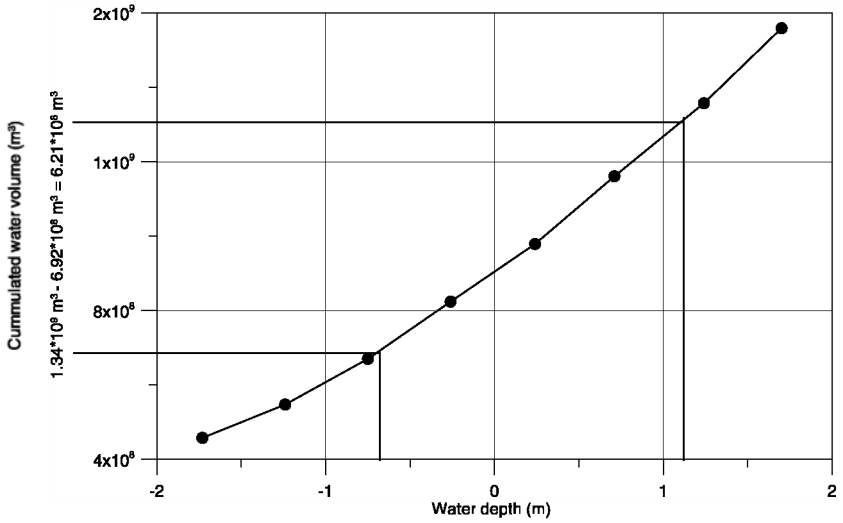


Fig. 5. Hypsographic curve used to determine the tidal prism for the Lister Dyb tidal area.

to export of sediment (Reise, 1998) or (more likely) that the techniques have been improved (e.g. more reliable bathymetry).

The fact that the current velocities and the deformation of the tidal wave are modelled satisfactorily makes the hydrodynamic simulation a good basis for the fine-grained sediment modelling.

### 4.2. Sedimentological conditions

In Fig. 6, matrix plots from the area are presented. The plots show suspended sediment concentrations at 2 days just before high water slack. Fig. 6A shows a typical situation under influence of wind blowing from east resulting in braking waves in the western part of the area, while Fig. 6B shows a situation with wind from the west with waves in the eastern part of the area. In Fig. 6A, it is seen that a relatively narrow band of concentrations around 500–700 mg $l^{-1}$ at the western part of the area is forming due to wave erosion. The broader band at the Jutland (eastern) side (Fig. 6B) is forming due to a lower bottom gradient, so that erosion due to breaking waves can take place over a larger area. A similar erosion pattern is also observed during field campaigns in the area where sediment concentrations at the tidal flats around high water can exceed 1000 mg $l^{-1}$ (Andersen, 1999). The suspended sediment concentrations measured during this study also show the highest values during onshore winds.

Fig. 7 shows time series of the suspended sediment concentrations at the two calibration sites for 7 days during the calibration period. The simulated sediment concentrations do not show a great similarity with the measured concentrations. However, the patterns of the modelled sediment concentrations are in accordance with the measured and expected patterns, thus, the highest concentrations are seen at low water slack and the lowest appears just after high water slack. At the intertidal parts of the area, it is seen that the characteristic pattern of high sediment concentrations just after and before drying of the flats appears.

An analysis comparing the sediment concentration patterns and wind statistics from the area shows that the sediment concentrations are very much dependent on the local wind conditions. The largest part of the area is showing the highest concentrations when the wind comes from the west and southwest, only the Kongsmark site is showing higher concentrations at easterly winds, which is onshore at the site. This is consistent with the findings of Andersen and Pejrup (2001), who found concentrations above 400 mg $l^{-1}$ during onshore winds, while the concentrations during offshore winds were between 50 and 250 mg $l^{-1}$. The sediment concentrations in the tidal channels are characterized by advection. Pejrup (1986) found that the sediment concentration patterns in the tidal channels are mostly determined by the wind direction, while the size of the concentrations is determined by the wind velocity. This is also the case in this study.

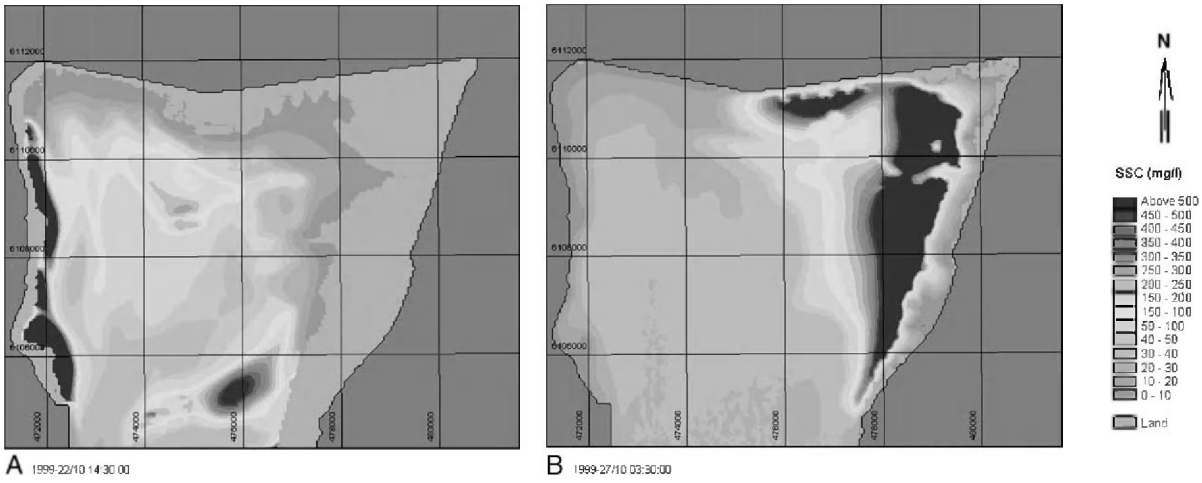


Fig. 6. Matrix plots showing simulated suspended sediment concentrations during easterly and westerly winds, respectively.

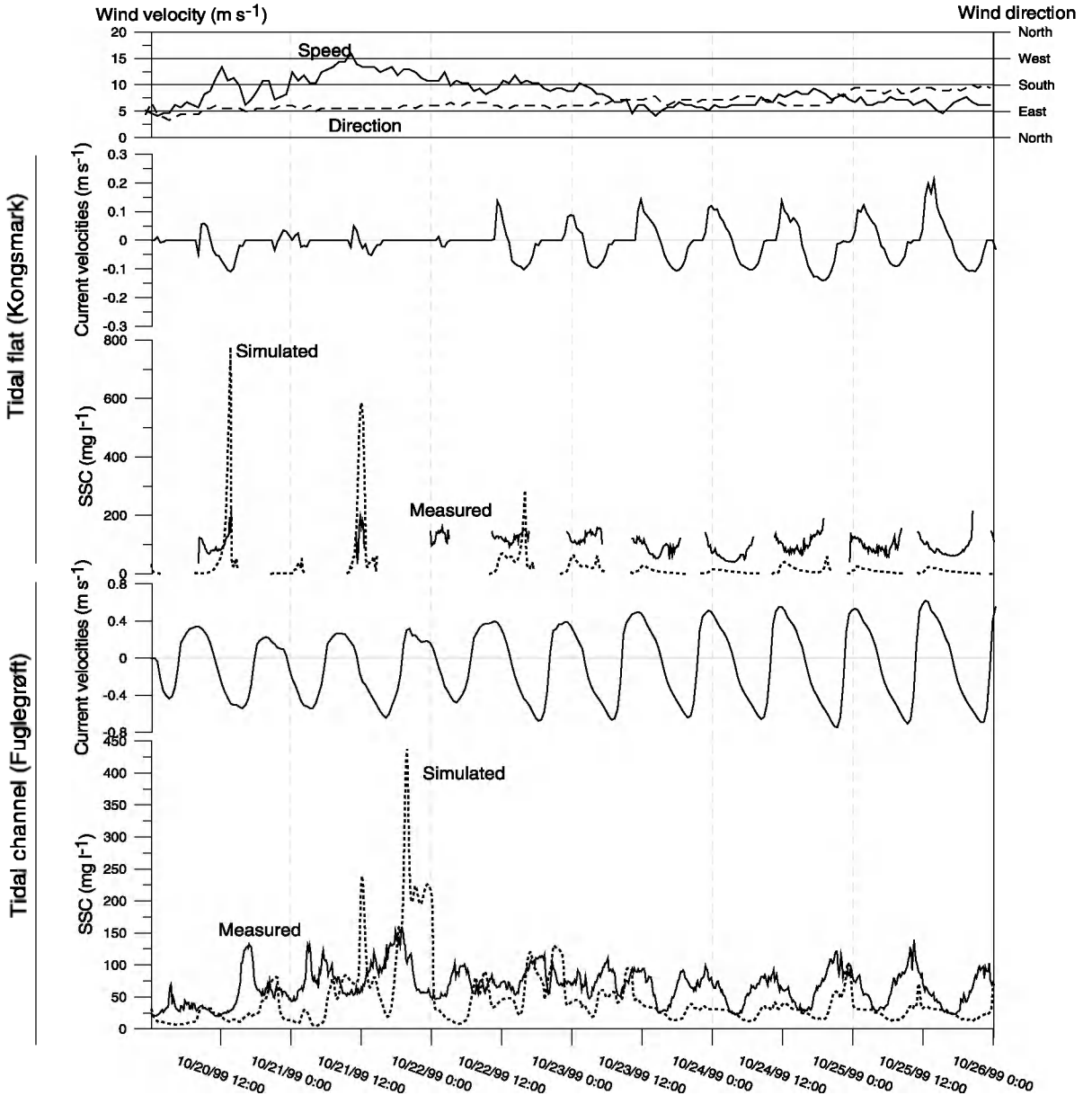


Fig. 7. Time series from the calibration phase showing measured and simulated suspended sediment concentrations and simulated current velocities at the calibration sites.

When onshore winds are prevailing, high sediment concentrations appear. This is related to wave activity, and generally, strong winds will erode the highest amount of sediment. However, during the investigated period, wind speeds around 8–12 m $s^{-1}$ are generating the highest sediment concentrations. This is speculated in a way so that strong winds are eroding more sediment from the bottom, but in the investigated period, these winds do not last long enough to mobilize sediment (wind speeds between 5 and 10 m $s^{-1}$ prevail 57% of the time while wind speeds over 15 m $s^{-1}$ only last 3% of the time). Therefore, in the

investigated area and period, the middle strong winds (8–12 m $s^{-1}$) are those which contribute to the highest degree of erosion.

At the intertidal flats, a typical concentration pattern with high concentrations just after inundation and before drying of the flat is recognized in some parts of the Rømø Dyb tidal area. This pattern is also observed by other authors (e.g. Andersen, 1999) and is connected to the low water depths and more influential wave activity, leading to higher bottom shear stresses.

Net sedimentation results from the Kongsmark site are shown in Fig. 8. It is seen that deposition in the order of 15–30 mm occurs in the beginning of the period. This coincides with easterly (onshore) light blowing winds, which gives import to the area. Then, a period of about 4 weeks follows, in which the sedimentation pattern shows a small export rate. This comes from northerly (longshore) and westerly (offshore) winds with low speeds. In the end of the simulation period, the wind is increasing to about 20 m $s^{-1}$ from the west. This results in a remarkably increase in the sedimentation, which may be due to the sheltering of the site and high sediment concentrations due to heavy wave activity in other parts of the area. In this area, mobilizing of sediment due to wave activity results in import of sediment to the inner areas.

Time series of the net sedimentation results show that sediment is transported inwards and settled in the tidal channels. When the next flood period appears, the sediment is eroded and brought further landwards. This makes an overall transport direction from the tidal channels toward the intertidal flats.

Andersen and Pejrup (2001) have carried out bed level measurements at three stations at Kongsmark during a 3-year period, 1997–2000. Results from these levellings, during the simulation period here presented, show a minor accretion at the most landward station and erosion in the order of a few centimeters at stations 225 and 575 m from land. Immediately after the simulation period has ended, Andersen and Pejrup (2001) observe accretion in the

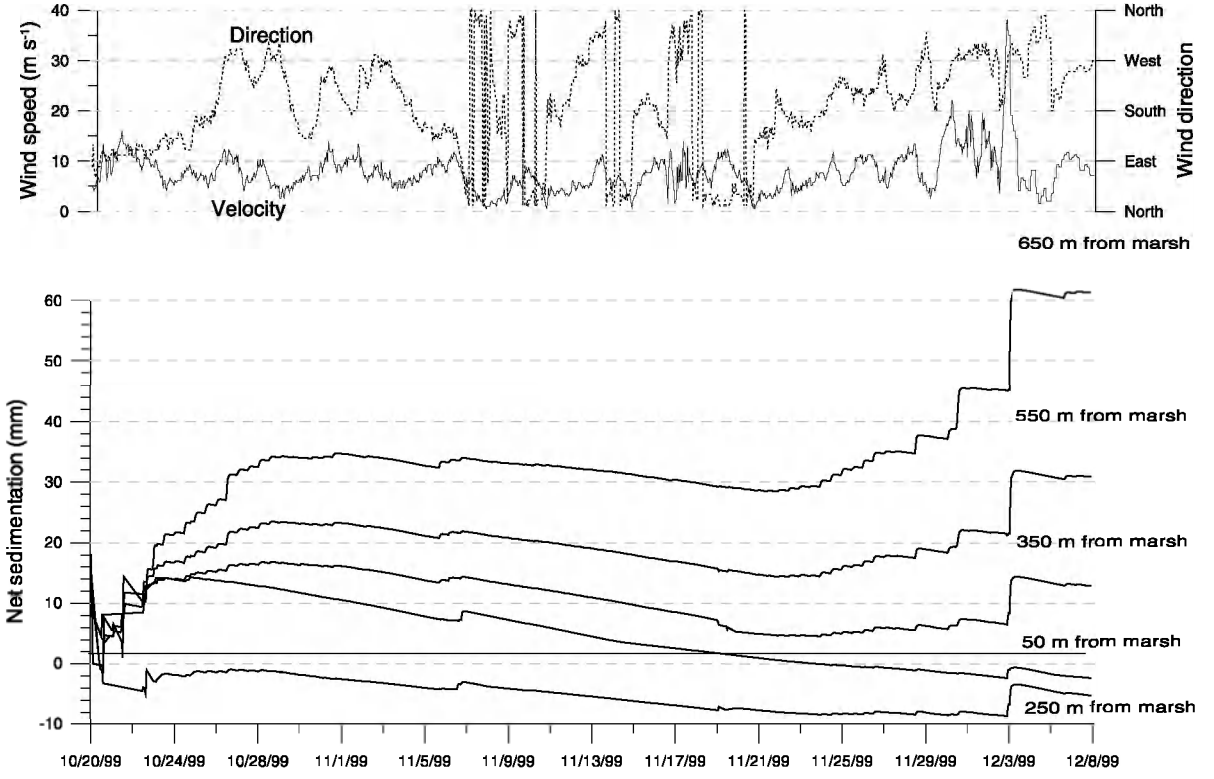


Fig. 8. Net sedimentation results from the Kongsmark site.

order of 2–10 cm. When these results are compared to the modelled net sedimentation presented in this paper, it is seen that the slight erosion occurring from October 30, 1999 to December 1, 1999 fits well with the bed level measurements from the period. Furthermore, the accretion measured after December 1, 1999 is also seen in the modelled results.

Generally, the simulations from the fine-grained sediment transport module show that the lowest concentrations appear around high water, while the highest concentrations appear at low water slack. The high concentrations at low water will tend to increase flocculation and thus leading to higher deposition rates. The newly deposited material will initially have a high erodibility. When the next flood period appears, the material will be moved landwards, resulting in an inward net transport direction.

The settling velocities of the sediments are a very important parameter when it comes to estimating the sedimentation in a specific estuary (Dyer, 1989; van Leussen, 1994; Van der Lee, 2000). For this reason, it has been tried to run several simulations using different settling velocities. The net sedimentation results from these simulations are shown in Fig. 9. It is remarkable that the description of settling velocities proposed by Burt (1986) and recommended by other authors (e.g. van Rijn, 1989) gives significantly lower net deposition rates than the findings from the Lister Dyb tidal area suggest.

Besides, the use of settling velocities collected during cold seasons gives lower deposition rates than using settling velocities collected during the summertime. This further emphasizes the importance of collecting site-specific settling velocities from the investigation area before setting up a cohesive sediment transport model or calculating deposition rates in any other way.

## 5. Conclusions

This study has focused on calibrating a numerical state-of-the-art model for computing water movements and cohesive sediment dynamics. The model

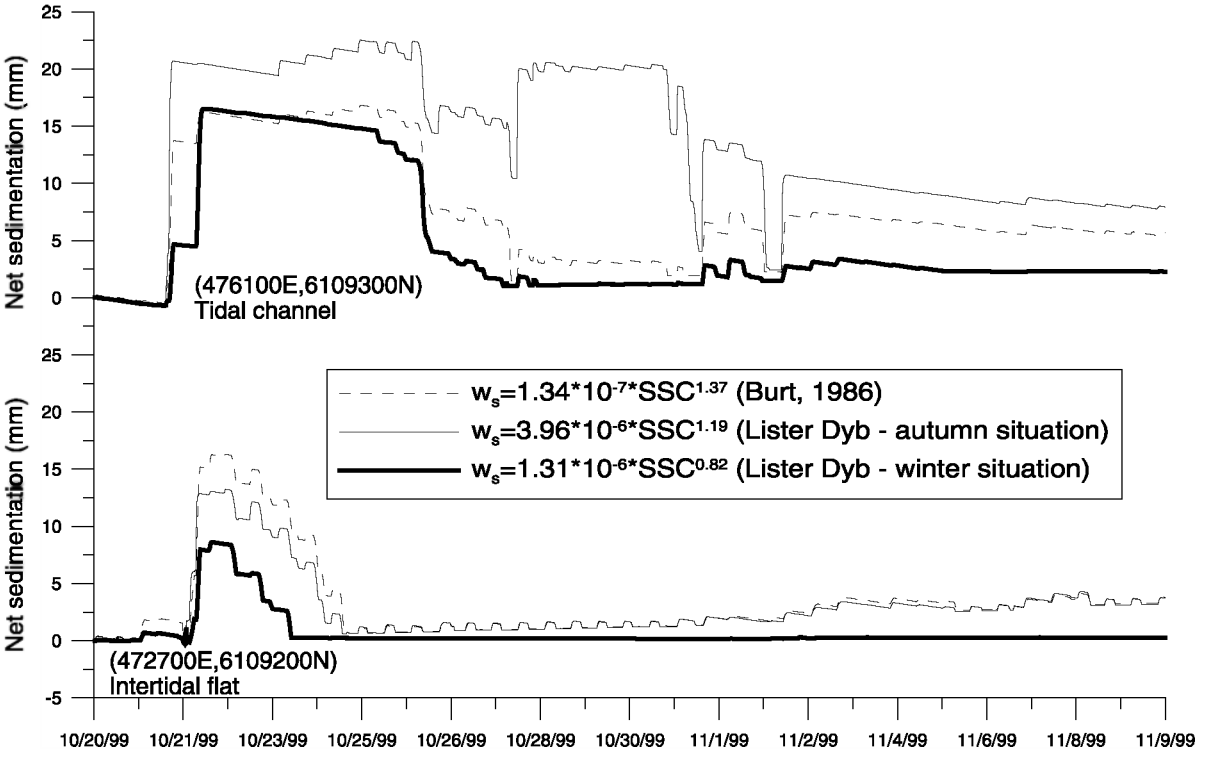


Fig. 9. Net sedimentation results from simulations using different settling velocities.

MIKE 21 MT has been used and a site-specific setup has been made with respect to sedimentological parameters in the area.

The hydrodynamic model covering the entire Lister Dyb tidal area has been validated against collected field data (Fig. 3). The model describes the actually occurring water movements in the area well and the deformation of the tidal wave is modelled satisfactorily (Fig. 4). It is a prerequisite that the hydrodynamic simulation is of high quality when cohesive sediment dynamics are to be modelled. Further, the study has established new and very reliable values for the tidal prism and current velocities in the area.

The magnitude of the modelled suspended sediment concentrations is in the same order of magnitude as reported in literature from the area (Pejrup et al., 1997; Andersen, 1999). The highest concentrations at a specific site appear when onshore winds are prevailing. This is speculated to be due to the wave activity in the area. The waves contribute with major influence to the bottom shear stresses especially in areas with low water levels like tidal mud flats. It is observed that the sediment settles out at low water slack and is eroded again at the flood tide. In accordance with the general concepts of settling and scour lag (van Straaten and Kuenen, 1958), the sediment will be transported in the flood direction and thus leading to an accretion of sediment in the inner parts of the area.

The net deposition rates have been compared to field measurements from the area (Andersen and Pejrup, 2001). The overall pattern shows concordance with the field measurements, but at some locations in the area, the deposition rates are frequently too high or occasionally too low. Using time series, it has been observed that the sediment transport from the tidal channels towards the intertidal flats is modelled satisfactorily.

During simulations that describe different scenarios for the settling velocity of the sediment, it has been shown that this single parameter can account for differences in accretion rates up to several centimetres each day. This further addresses the need for a site-specific model setup. A setup that is not site-specific can lead to insignificant or even wrong results.

Through this study, it has been shown that it is possible to model cohesive sediment transport in a highly dynamic area like a tidal influenced estuary. The properties of the fine-grained sediments are very complex and difficult to describe theoretically. Although modelling of cohesive sediment transport is a complicated task, it is, through a site-specific setup, possible to get right orders and patterns of suspended sediment concentrations and net sedimentations.

## Acknowledgements

The authors would like to thank "DHI-Water and Environment" for kindly providing the software used (MIKE 21). Karen Edelvang, Morten Pejrup and Thorbjørn Joest Andersen are thanked for helpful discussions and assistance during fieldwork. Klavs Bundgaard and Thomas Uhrenholdt from "DHI-Water and Environment" are thanked for technical assistance during the model setup. The comments from two anonymous reviewers are highly appreciated.

## Appendix A

Nomenclature

| | | |
|---|---|---|
| $\alpha$ | m $N^{-0.5}$ | $\alpha$ coefficient |
| $\beta$ | | Angle between the mean current direction and the direction of wave propagation |
| $\tau_b$ | N $m^{-2}$ | Shear stress at the bottom |
| $\tau_{cd}$ | N $m^{-2}$ | Critical bottom shear stress for deposition |
| $\tau_{ce}$ | N $m^{-2}$ | Critical bottom shear stress for erosion |
| $a$ | m | The horizontal mean wave orbital motion at the bed |
| $c$ | mg $l^{-1}$ | Depth averaged suspended sediment concentration |
| $D_{max}$ | $m^2$ $s^{-1}$ | Maximum dispersion coefficient |
| $D_{min}$ | $m^2$ $s^{-1}$ | Minimum dispersion coefficient |
| $D_X$, $D_Y$ | $m^2$ $s^{-1}$ | Dispersion coefficient in X and Y directions |
| $E$ | g $m^{-2}$ $s^{-1}$ | Bed erodibility |
| $k$ | | Empirical constant in the settling velocity equation |
| $k_b$ | m | Bed roughness |
| $m$ | | Settling index |
| $Q_{max}$ | $m^3$ $s^{-1}$ | Maximum water transport |
| $T_i$ | g $m^{-2}$ $s^{-1}$ | Transition coefficient |
| $U_b$ | m $s^{-1}$ | Horizontal mean wave orbital velocity at the bed |
| $U_\delta$ | m $s^{-1}$ | Current velocity at the top of wave boundary layer |

| | | |
|---|---|---|
| $V_{50}$ | m s$^{-1}$ | Mean current velocity |
| $V_{max}$ | m s$^{-1}$ | Maximum current velocity |
| $w_s$ | m s$^{-1}$ | Settling velocity of sediment |
| $z_0$ | m | Bed resistance |

## References


Andersen, T.J., 1999. Suspended sediment transport and sediment reworking at an intertidal mudflat, the Danish Wadden Sea. Meddelelser fra Skalling-Laboratoriet 37, 1–72.

Andersen, T.J., Pejrup, M., 2001. Suspended sediment transport on a temperate, microtidal mudflat, the Danish Wadden Sea. Marine Geology 173, 69–85.

Austen, I., Andersen, T.J., Edelvang, K., 1999. The influence of benthic diatoms and invertebrates on the erodibility of an intertidal mudflat, the Danish Wadden sea. Estuarine, Coastal and Shelf Science 49, 99–111.

Backhaus, J., Hartke, D., Hübner, U., Lohse, H., Müller, A., 1998. Hydrographie und Klima im Lister Tidebecken. In: Gätje, C., Reise, K. (Eds.), Ökosystem Wattenmeer-Austausch, Transport-und Stoffumwandlungsprozesse, Chap. 1.1.3. Springer, Heidelberg, pp. 39–54. In German.

Bayerl, K., Köster, R., Murphy, D., 1998. Verteilung und Zusammensetzung der Sedimente im Lister Tidebecken. In: Gätje, C., Reise, K. (Eds.), Ökosystem Wattenmeer-Austausch, Transport-und Stoffumwandlungsprozesse, Chap. 1.1.2. Springer, Heidelberg, pp. 31–38. In German.

Burt, N., 1986. Field settling velocities of estuary muds. In: Mehta, A.J. (Ed.), Estuarine Cohesive Sediment Dynamics, vol. 14. Springer, Berlin, pp. 126–150. Chap. 7.

Cancino, L., Neves, R., 1999. Hydrodynamic and sediment suspension modelling in estuarine systems: Part II. Application to the Western Scheldt and Gironde estuaries. Journal of Marine Systems 22, 117–131.

Davies, J.L.H., 1964. A morphogenetic approach to world shorelines. Zeitschrift der Geomorphologie 8, 127–142.

DHI, 1999a. MIKE 21 hydrodynamic module. User guide and reference manual, Release 2.7.

DHI, 1999b. MIKE 21 near shore waves module. User guide and reference manual, Release 2.7.

Dyer, K., 1989. Sediment processes in estuaries: future research requirements. Journal of Geophysical Research 94, 14327–14339.

Edelvang, K., 1996. The significance of particle aggregation in an estuarine environment. Case studies from the Lister Dyb Tidal area. Geographica Hafniensia, A 5, 1–105.

Eisma, D., 1998. Intertidal Deposits; River Mouths, Tidal Flats and Coastal Lagoons. CRC Press LLC, London.

Fanger, H.U., Backhaus, J., Hartke, D., Hübner, U., Kappenberg, J., Müller, A., 1998. Hydrodynamik im Lister Tidebecken. In: Gätje, C., Reise, K. (Eds.), Ökosystem Wattenmeer-Austausch, Transport-und Stoffumwandlungsprozesse, Chap. 2.3.1. Springer, Heidelberg, pp. 161–184. In German.

Hayes, M.O., 1979. Barrier island morphology as a function of tidal and wave regime. In: Leatherman, S.P. (Ed.), Barrier Islands. Academic Press, New York, pp. 1–27.

Holthuijsen, L.H., Booij, N., Herbers, T.H.C., 1989. A prediction model for stationary, short-crested waves in shallow water with ambient currents. Coastal Engineering 13, 23–54.

Janssen-Stelder, B., 2000. The effect of different hydrodynamic conditions on the morphodynamics of a tidal mudflat in the Dutch Wadden Sea. Continental Shelf Research 20, 1461–1478.

Johnson, H.K., 1998. On modelling wind-waves in shallow and fetch limited areas using the method of Holthuijsen, Booij and Herbes. Journal of Coastal Research 14, 917–932.

Krone, R.B., 1962. Flume Studies of the Transport of Sediment in Estuarine Shoaling Processes. Final Report to San Francisco District US Army Corps of Engineers, Washington DC. University of California, Berkeley.

Le Normant, C., 2000. Three-dimensional modelling of cohesive sediment transport in the Loire estuary. Hydrological Processes 14, 2231–2243.

Lundbak, A., 1945. Det Sydvestjydske Vadehavs Hydrografi (In Danish).

Mehta, A.J., Partheniades, E., 1975. An investigation of the depositional properties of flocculated fine sediments. Journal of Hydraulic Research 12, 361–381.

Mehta, A.J., Hayter, E.J., Parker, W.R., Krone, R.B., Teeter, A.M., 1989. Cohesive sediment transport: Part I. Process description. Journal of Hydraulic Engineering, ASCE 115, 1076–1093.

Mikkelsen, O.A., Pejrup, M., submitted for publication. Factors controlling the in situ settling velocity of cohesive sediment in estuaries. Submitted to Journal of Sea Research.

Møller, A.L., Mikkelsen, O.A., 1997. Vertikal og horisontal transport og fordeling af suspenderet sediment-sammenlignende metodestudier fra Lister Dybs tidevandsområde og et kystnært vandlegeme i Nordsøen. Unpublished master thesis (in Danish).

Parchure, T.M., Mehta, A.J., 1985. Erosion of soft cohesive sediment deposits. Journal of Hydraulic Engineering, ASCE 111, 1308–1326.

Parker, W.R., 1997. On the characterization of cohesive sediment for transport modelling. In: Burt, N., Parker, R., Watts, J. (Eds.), Cohesive Sediments, Chap. 1. Wiley, Chichester, pp. 3–15.

Pejrup, M., 1986. Parameters affecting fine-grained suspended sediment concentrations in a shallow micro-tidal estuary, Ho Bugt, Denmark. Estuarine, Coastal and Shelf Science 22, 241–254.

Pejrup, M., 1988. Flocculated suspended sediment in a micro-tidal environment. Sedimentary Geology 57, 249–256.

Pejrup, M., Edelvang, E., 1996. Measurements of in situ settling velocities in the Elbe estuary. Journal of Sea Research 36, 109–113.

Pejrup, M., Larsen, M., Edelvang, K., 1997. A fine-grained sediment budget for the Sylt–Rømø tidal basin. Helgoländer Meeresuntersuchungen 51, 253–268.

Perillo, G.M.E., 1995. Definitions and geomorphologic classifications of estuaries. In: Perillo, G.M.E. (Ed.), Geomorphology and Sedimentology of Estuaries. Elsevier, pp. 17–47.

Postma, H., 1981. Exchange of materials between the North Sea and the Wadden Sea. Marine Geology 40, 199–213.

Pritchard, D.W., 1960. Lectures on estuarine oceanography. In: Kinsman, B. (Ed.), Johns Hopkins University, 154 pp.

Rae, J.E., 1997. Trace metals in deposited intertidal sediments. In: Jickells, T.D., Rae, J.E. (Eds.), Biogeochemistry of Inter-

tidal Sediments, vol. 9. Cambridge Univ. Press, Cambridge, pp. 16–41. Chap. 2.

Reise, K., 1998. Coastal change in a tidal backbarrier basin of the North Wadden Sea: are tidal flats fading away? Senckenbergiana Maritima 29, 121–127.

Teeter, A.M., 1986. Vertical transport in fine-grained suspension and newly deposited sediment. In: Mehta, A.J. (Ed.), Estuarine Cohesive Sediment Dynamics, vol. 14. Springer, Berlin, pp. 170–191. Chap. 9.

Teisson, C., 1991. Cohesive suspended sediment transport: feasibility and limitations of numerical modelling. Journal of Hydraulic Research 29, 755–769.

Teisson, C., 1997. A review of cohesive sediment transport processes. In: Burt, N., Parker, R., Watts, J. (Eds.), Cohesive Sediments, Chap. 26. Wiley, Chichester, pp. 367–381.

Van der Lee, W.T.B., 2000. The settling of mud flocs in the Dollard estuary, The Netherlands. Netherlands Geographical Studies 274, 15–121.

van Leussen, W., 1994. Estuarine macroflocs and their role in fine-grained sediment transport. PhD thesis, University of Utrecht, The Netherlands, 488 pp.

van Rijn, L.C., 1989. Transport of cohesive materials. Delft Hydraulics H 461, 12.1–12.27.

van Straaten, L.M.J.U., Kuenen, P.H., 1958. Tidal action as a cause of clay accumulation. Journal of Sedimentary Petrology 28, 406–413.